

Detection of Shape Deformities using Yamabe flow and Beltrami coefficients

*Lok Ming Lui^{1,2}, Tsz Wai Wong², Wei Zeng⁴, Xianfeng Gu⁴
Paul M. Thompson³, Tony F. Chan^{2,5} AND Shing Tung Yau¹*

¹ Department of Mathematics, Harvard University

² Department of Mathematics, UCLA

³ Laboratory of Neuro Imaging, UCLA Medical School

⁴ Department of Computer Science, Stony Brook University

⁵ Hong Kong University of Science and Technology

Abstract

We address the problem of detecting deformities on elastic surfaces. This is of great importance for shape analysis, with applications such as detecting abnormalities in biological shapes (e.g., brain structures). We propose an effective algorithm to detect abnormal deformations by generating quasi-conformal maps between the original and deformed surfaces. We firstly flatten the 3D surfaces conformally onto 2D rectangles using the discrete Yamabe flow and use them to compute a quasi-conformal map that matches internal features lying within the surfaces. The deformities on the elastic surface are formulated as non-conformal deformations, whereas normal deformations that preserve local geometry are formulated as conformal deformations. We then detect abnormalities by computing the Beltrami coefficient associated uniquely with the quasi-conformal map. The Beltrami coefficient is a complex-valued function defined on the surface. It describes the deviation of the deformation from conformality at each point. By considering the norm of the Beltrami coefficient, we can effectively segment the regions of abnormal changes, which are invariant under normal (non-rigid) deformations that preserve local geometry. Furthermore, by considering the argument of the Beltrami coefficient, we can capture abnormalities induced by local rotational changes. We tested the algorithm by detecting abnormalities on synthetic surfaces, 3D human face data and MRI-derived brain surfaces. Experimental results show that our algorithm can effectively detect abnormalities and capture local rotational alterations. Our method is also more effective than other existing methods, such as the isometric indicator, for locating abnormalities.

I. INTRODUCTION

Detecting abnormal changes on surfaces is a central problem in shape analysis, especially in medical research. For example, neuroscientists commonly aim to identify abnormal deformations of cortical and subcortical structures in the brain in order to detect systematic patterns of alterations in brain diseases. In cardiac imaging and oncology, physicians commonly need to track changes or abnormalities in biological organs or tumors, to evaluate the effectiveness of different treatments, or monitor disease progression. Detecting and examining abnormalities with the human eye is inefficient and often inaccurate, especially on complicated surfaces such as the cerebral cortex of the brain. Therefore, it is of great importance to develop automatic methods to detect abnormalities and track abnormal geometric changes over time.

In this paper, we propose a framework for detecting abnormal changes on elastic surfaces using quasi-conformal geometry. Two issues arise in solving this problem. First, we want to find good registrations between surfaces with enforced landmark-correspondences. Second, we want to define a robust measure of deformity, which is invariant under normal (non-rigid) deformations that preserve local geometry, so that quantitative analysis can be carried out. These goals are related, since good registrations allow accurate detection of abnormalities, while good measures of deformity can be used to set criteria for desirable registrations.

We propose to model deformities between elastic shapes as non-conformal deformations, whereas normal deformations that preserve the local geometry are formulated as conformal deformations. This is a generalization of existing work by Lord et al. and Unal et al. [9] [19], which modeled deformities between shapes as non-isometric diffeomorphisms. Using the isometric indicator, the authors proposed to detect abnormalities that are invariant under rigid transformations. Our proposed method is an extension of their approaches, in that we are trying to detect deformities on elastic surfaces that are invariant under non-rigid normal deformations. This is a more general and accurate definition in some situations. For example, we may consider the growth processes of the human body, which is a key area of study in medical imaging and face recognition. As a person grows, different parts of the human body grow locally and the growth rate is somewhat uniform locally [17]. The same organs of two healthy individuals tend to have similar shapes, although they may not be exactly isometric to each other. In other words, local geometry is well preserved under the normal growth process. Conformal maps are well-known to preserve local geometry. Therefore, a good registration between two organs of the same or different individuals should not be far from conformal. This motivates us to define good registrations as conformal registrations, and measure deformities as regions of non-conformality.

The key contribution in this paper is the use of Beltrami coefficient to detect shape abnormalities. Suppose we are given a registration between a normal and a deformed surface of the same or different subjects. We can compute the Beltrami coefficient of the registration map, which is a complex-valued function measuring the non-conformal deformation at each point of the map. In our examples, we show that the Beltrami coefficient is an effective measure of shape deformities on elastic surfaces.

To complete our framework for the automatic detection of shape deformities, we propose the following registration algorithm. We first generate a quasi-conformal map between the original 3D surface and the surface to be compared with it. The surfaces are first conformally flattened onto 2D rectangles using a novel Yamabe flow method, which computes accurate conformal parameterizations of surfaces. Then, a quasi-conformal map is computed to match landmark features between both flattened surfaces. By formulating abnormal changes as non-conformal deformations, we detect abnormalities by computing the Beltrami coefficient, which is uniquely associated with the quasi-conformal map. By considering the norm of the Beltrami coefficient, we detect regions with abnormal changes, which are invariant under conformal deformation. Furthermore, by considering the argument of the Beltrami coefficient, we can capture abnormalities induced by local rotational changes. We propose a quantity called the Beltrami index, which allows us to quantitatively describe the degree of abnormality in each region. Experiments

applying our algorithm to synthetic surfaces, 3D human face data and real MRI-derived brain surfaces show that our algorithm can effectively detect abnormalities and capture local rotational alterations. The algorithm is also robust under added noise, and it is successful in detecting altered gyrification patterns on cortical surfaces. Quantitative comparisons of the size of abnormality with the Beltrami index show that the detected sizes of abnormalities correspond positively with the sizes of abnormalities. A comparison of the Beltrami coefficient with other commonly used measures like the isometric indicator and gradient show that these measures are not as effective as Beltrami coefficient and may tend to give misleading results when the compared surfaces undergo normal changes that preserve the local geometry.

Our paper is organized as follows: prior work on related topics is presented in section 2. The basic mathematical theory is discussed in section 3. In Section 4, the details of our proposed model are discussed. In Section 5, our computer algorithm is summarized. Experimental results are discussed in Section 6, and some conclusions and future work are discussed in section 7.

II. PREVIOUS WORK

Many different approaches have been proposed to detect changes in shapes. Most of them take into account properties that depend on the embedding of the shape in space. Tosun et al. [18] proposed the use of three different shape measures – the shape index, curvedness, and L2 norm of mean curvature – to quantify cortical gyrification and complexity. While the curvature measure is an important geometric measure of surface properties, it is also affected by healthy changes like normal growth, which increases surface size and decreases curvature. Moreover, since the curvature is a second order geometric measure, it is more sensitive to noise in data, especially in triangular meshes. Extra preprocessing is required to guarantee the robustness of the measure. In contrast, the Beltrami coefficient we use in this paper is a first order geometric measure. This leads to less perturbation due to noise. By computing surface Jacobian and applying statistical inference via random field theory on cortical surfaces processed by diffusion smoothing, Chung et al. [2] studied changes in cortical surface area, thickness, and curvature, as well as the change of the total gray matter volume over time. While surface Jacobian can detect area changes caused by abnormalities, it can also be affected by healthy deformations like normal growth, which also causes area changes of surface registrations. By looking at the Beltrami coefficients, we are able to minimize the effects caused by such changes. We are also able to detect rotational distortions caused by abnormalities. Shi et al. [15] suggested the use of Hamilton-Jacobi skeletons on cortical surfaces to study gyrification patterns in Williams syndrome. In this approach, the degree of gyrification is measured by the number of branches in the Hamilton-Jacobi skeleton. While this method is easily computable and gives a fast measure of complexity of the cortical surface, subtle changes could occur within a branch of the cortical surface, which require a finer measure to detect. To overcome this problem, our approach provides an local and intrinsic measure of surface distortion to detect such changes.

Registration is broadly used in medical imaging and face recognition. It aims to produce a desirable registration for obtaining good correspondences or performing further analysis. Grenander et al. [4] surveyed existing methods of computational anatomy and proposed a framework to compute deformation

maps and empirical probability laws for disease testing. Early work such as Gaser et al. [3] compute an initial correspondence field between surfaces to ease the detection of abnormalities. Such applications often involve models of the human face or organs of the human body. Some existing methods model deformities between shapes in terms of nonrigid or non-isometric diffeomorphisms [9] [19]. This may make their algorithms classify normal growth in living organisms as abnormal. This motivates us to model abnormalities as non-conformal diffeomorphisms, and good registrations as ones that are as conformal as possible. We support our view with the following points. First, normal changes such as growth in humans tend to preserve local geometry well, and hence are conformal. Second, by modeling good registrations as those that are conformal, we are still able to get a correct registration when the proper registration is indeed isometric.

In most methods for detecting shape changes, an accurate registration between two shapes has to be computed. The area has been extensively studied. Unal et al. [19] proposed the use of coupled PDEs for joint segmentation and registration. However, technique does not support the matching of user-defined landmarks. Pohl et al. [14] proposed an expectation maximization-based method to solve the problem, which takes into account of image artifacts, anatomical labelmaps, and a structure-dependent hierarchical mapping from the atlas to the image space. This allows some controls over the matched areas, but user-defined landmark constraints may not be matched. Lord et al. [9] [8] proposed to match hippocampal surfaces by finding maps minimizing the deviation from isometry under the constraints of piecewise deformation homogeneity, with local asymmetry quantified. The authors defined asymmetries between paired shapes as non-rigid diffeomorphisms between shapes. However, under normal conditions, like growth, non-rigid shape changes naturally occur. In one of our examples, it is shown that the maps of a correctly matched pair of surfaces can be non-isometric in normal as well as abnormal regions. Such occasions call for a more flexible definition of shape abnormality.

It has become increasingly popular to study shape changes by computing diffeomorphisms with desired properties, as they give one-to-one correspondences of shapes for local comparisons. Using control theory and large-deformation continuum mechanics, variational metrics have been developed on the space of diffeomorphisms [4] [20]. In computing diffeomorphisms, one of the goals is to preserve local geometry as far as possible while consistently aligning important anatomical features lying within a surface. Gu et al. [6] proposed to find an optimal Möbius transformation between two surfaces to minimize a landmark mismatch error. Wang et al. [21][11] defined a new energy functional based on harmonic energy to optimize the conformal parameterization of cortical surfaces, while fixing landmark correspondences. The harmonic energy method was applied by Shi et al. [16] to match implicitly-defined surfaces by solving PDEs on them using level set methods. Using integral flows of smooth vector fields, Lui et al. [10] further proposed to compute a landmark-matching diffeomorphism with shape-based correspondences between landmark curves.

Recently, conformal geometry has been used for 3D non-rigid surface matching and registration. Harmonic maps have been used to track non-rigid motions of 3D surfaces, which requires tracking of boundary correspondences. This challenge was addressed in [23][25], where different conformal mappings

induced by different holomorphic differentials were combined to achieve accurate and robust matching results. Even so, holomorphic differentials cannot handle surfaces with complicated topology; the Ricci flow method is much more flexible and general. The surface-based Ricci flow was introduced in [7]. The theory of discrete surface Ricci flow was introduced in [1]. Euclidean Ricci flow has been applied to 3D shape analysis in [5], where all the Gaussian curvatures of the surface are concentrated on several singularities. To remove these singularities, the discrete hyperbolic Ricci flow was introduced in [22], which improves the accuracy and robustness of the matching and registration. In practice, the Ricci flow method imposes constraints on the triangulation of the discrete surface, whereas the discrete Yamabe flow can handle much more general triangulations. Furthermore, the Yamabe flow can achieve a higher level of conformality than the Ricci flow. The theory of discrete Yamabe flow is established in [12], where the existence, uniqueness and stability of the solution is rigorously proven.

III. MATHEMATICAL BACKGROUND

In this section, we describe some basic mathematical concepts relevant to describing our algorithm.

A surface S with a conformal structure is called a *Riemann surface*. Given two Riemann surfaces M and N , a map $f : M \rightarrow N$ is *conformal* if it preserves the surface metric, up to a multiplicative factor called the *conformal factor*. An immediate consequence is that every conformal map preserves angles. With the angle-preserving property, a conformal map effectively preserves the local geometry of the surface structure.

A generalization of conformal map is called the *quasi-conformal* map which is an orientation-preserving homeomorphism between Riemann surfaces with bounded conformality distortion, in the sense that the first order approximation of the quasi-conformal homeomorphism takes small circles to small ellipses of bounded eccentricity. Thus, a conformal homeomorphism that maps a small circle to a small circle can also be regarded as quasi-conformal. Mathematically, f is quasi-conformal provided that it satisfies the Beltrami's equation:

$$\frac{\partial f}{\partial \bar{z}} = \mu(z) \frac{\partial f}{\partial z} \quad (1)$$

for some complex-valued Lebesgue-measurable μ satisfying $|\mu|_\infty < 1$. In terms of the metric tensor, consider the effect of the pullback under f of the usual Euclidean metric ds_E^2 ; the resulting metric is given by:

$$f^*(ds_E^2) = \left| \frac{\partial f}{\partial z} \right|^2 |dz + \mu(z)d\bar{z}|^2 \quad (2)$$

which, relative to the background Euclidean metric dz and $d\bar{z}$, has eigenvalues $(1+|\mu|)^2 \frac{\partial f}{\partial z}$ and $(1-|\mu|)^2 \frac{\partial f}{\partial \bar{z}}$. μ is called the *Beltrami coefficient*, which is a measure of conformality. In particular, the map f is conformal around a small neighborhood of p when $\mu(p) = 0$. Also, the gradient and the Beltrami coefficient of the map are closely related. Suppose $f = (f_1, f_2)$ under the conformal parameter domains. The Jacobian matrix J of f can be written as $(\nabla f_1, \nabla f_2)$ which is a 2×2 matrix. The Jacobian is closely related to $|\mu_f|$. Mathematically,

$$\det(J) = (1 - |\mu_f|^2)(|\nabla f_1|^2 + |\nabla f_2|^2 + \det(J))/4$$

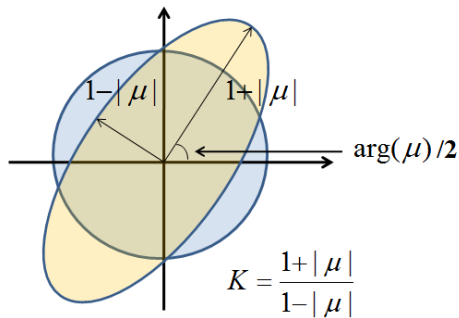


Fig. 1. Illustration of how Beltrami coefficient μ measures the distortion by a quasi-conformal mapping that maps a small circle to an ellipse with dilation K .

While $|\det(J)|$ gives us information about the area distortion under the map f , $|\mu_f|$ gives us information about the conformality distortion. In other words, $|\mu_f|$ measures the regions of deformations that do not preserve local geometry.

Infinitesimally, around a point p , f may be expressed with respect to its local parameter as follows:

$$\begin{aligned} f(z) &= f(p) + f_z(p)z + f_{\bar{z}}(p)\bar{z} \\ &= f(p) + f_z(p)(z + \mu(p)\bar{z}) \end{aligned} \quad (3)$$

Obviously, f is not conformal if and only if $\mu(p) \neq 0$. Inside the local parameter domain, f may be considered as a map composed of a translation of $f(p)$ together with a stretch map $S(z) = z + \mu(p)\bar{z}$, which is postcomposed by a multiplication of $f_z(p)$ which is conformal. All the conformal distortion of $S(z)$ is caused by $\mu(p)$. $S(z)$ is the map that causes f to map a small circle to a small ellipse. From $\mu(p)$, we can determine the angles of the directions of maximal magnification as well as the amount of maximal magnification and maximal shrinking. Specifically, the angle of maximal magnification is $\arg\mu(p)/2$ with magnifying factor $1 + |\mu(p)|$; the angle of maximal shrinking is the orthogonal angle $(\arg\mu(p) - \pi)/2$ with shrinking factor $1 - |\mu(p)|$. The distortion or dilation is given by:

$$K = \frac{1 + |\mu(p)|}{1 - |\mu(p)|} \quad (4)$$

Thus, the Beltrami coefficient μ gives us all the information about the conformality of the map (See Figure 1). This motivates its use as a measure of abnormal deformation, as abnormalities tend to cause significant distortions in the conformality of the deformation map.

It is often convenient to conformally map 3D surfaces to planar domains, to simplify subsequent computations. Yamabe flow offers a rigorous and efficient way to do this. Suppose S is a surface embedded in the 3D Euclidean space \mathbb{R}^3 , then it has the induced Euclidean metric denoted by $\mathbf{g} = (g_{ij})$. Let $u : S \rightarrow \mathbb{R}$ be a function on S , then $\bar{\mathbf{g}} = e^{2u}\mathbf{g}$ is another Riemannian metric of S , which is conformal to \mathbf{g} . If the Gaussian curvatures induced by \mathbf{g} and $\bar{\mathbf{g}}$ are K and \bar{K} , then they are related by the following *Yamabe equation*

$$\bar{K} = e^{2u}(-\Delta_{\mathbf{g}}u + K), \quad (5)$$

where $\Delta_{\mathbf{g}}$ is the Laplace-Beltrami operator under the original metric \mathbf{g} .

It is fundamentally important to design a Riemannian metric \bar{g} with a prescribed curvature \bar{K} , which is equivalent to solving the Yamabe equation. The surface Yamabe flow (or equivalently the Ricci flow) is a powerful tool for solving it. Intuitively, the surface Yamabe flow deforms the metric in proportion to the Gaussian curvature, such that the Gaussian curvature evolves according to a heat diffusion process.

$$\frac{dg_{ij}}{dt} = (\bar{K} - K)g_{ij}. \quad (6)$$

It has been proven [12] that if $\bar{K} \equiv 0$ everywhere and the total area is preserved during the flow, the Yamabe flow converges and leads to a metric with constant Gaussian curvature. Note that, for higher-dimensional Riemannian manifolds, the Ricci flow and Yamabe flow are different. On discrete surfaces, the discrete Yamabe flow produces better conformality than the discrete Ricci flow.

IV. OUR PROPOSED MODEL

In our method, we propose to use the Beltrami coefficient to detect abnormalities on surfaces. This is done by formulating abnormal changes as non-conformal deformations. Conversely, a conformal deformation is considered as normal. This definition is based on the fact that the local geometries of shape are well-preserved under normal changes, such as biological shape deformations. Conformal maps are well known to preserve local geometry and thus it is plausible to use them to characterize normal deformation. When shapes undergo abnormal changes, significant local distortions in conformality are often observed. This motivates us to consider the Beltrami coefficient, which measures the degree of conformality distortion, for abnormality detection. Our proposed algorithm has three main steps. First, the original 3D surface and the deformed surface are conformally parameterized onto 2D rectangles using the Yamabe flow method. This simplifies the problem by transforming the 3D surface problem into a 2D problem. Second, a quasi-conformal map is obtained between the two surfaces by computing a harmonic map between their conformal parameter domains, which also accommodates constraints to match internal landmarks based on their shapes. This gives a one-to-one correspondence (registration) between the two surfaces. Finally, the Beltrami coefficient associated with the quasi-conformal map is computed as an index of abnormal changes. We describe each step in detail next.

A. Conformal parameterization using the Yamabe Flow

To detect regions with abnormalities, the first step is to find a one-to-one correspondence (registration) between the original and deformed surfaces. With this registration, we can detect the distortion in conformality of the deformation at each point by computing the associated Beltrami coefficient. Computing the surface registration directly on surfaces is difficult, especially on complicated surfaces such as the cortical surface of the brain. Therefore, it is advantageous for us to first parameterize the surfaces conformally onto the 2D parameter domain. This simplifies the process by transforming the surface problem into a 2D problem. Under the conformal parameterizations, determining conformality distortion between surfaces is equivalent to determining it between their conformal parameter domains. Of course, the computation of conformal parameterizations has to be accurate in order to effectively detect changes in conformality. The Yamabe flow (6) provides us with an efficient and accurate way to compute these conformal maps.

In practice, all surfaces are approximated by piecewise linear triangular meshes $M(V, E, F)$, where V , E and F represent the vertex, edge and face set of the mesh. We use v_i to denote the i -th vertex, $[v_i, v_j]$ the edge connecting v_i and v_j , $[v_i, v_j, v_k]$ the face connecting v_i, v_j, v_k . The *discrete metric* is the edge length function $\ell : E \rightarrow \mathbb{R}^+$ satisfying triangle inequality. The *vertex discrete curvature* is defined as angle deficiency,

$$K_i = \begin{cases} 2\pi - \sum_{[v_i, v_j, v_k] \in F} \theta_i^{jk} & v_i \notin \partial M \\ \pi - \sum_{[v_i, v_j, v_k] \in F} \theta_i^{jk} & v_i \in \partial M \end{cases}$$

where θ_i^{jk} is the corner angle at v_i in the face $[v_i, v_j, v_k]$, ∂M is the boundary of M . Let $\mathbf{u} : V \rightarrow \mathbb{R}$ be the discrete conformal factor. The edge length of $[v_i, v_j]$ is defined as

$$\ell_{ij} := \exp(u_i) \exp(u_j) \ell_{ij}^0,$$

where ℓ_{ij}^0 is the original edge length in \mathbb{R}^3 . The discrete Yamabe flow is defined as

$$\frac{du_i}{dt} = \bar{K}_i - K_i,$$

with the constraint $\sum_i u_i = 0$. The discrete Yamabe flow converges, and the final discrete metric induces the prescribed curvature; a detailed proof can be found in [12]. The discrete Yamabe flow is the negative gradient flow of the following *Yamabe energy*,

$$E(\mathbf{u}) = \int_{\mathbf{u}_0}^{\mathbf{u}} \sum_i (\bar{K}_i - K_i) du_i,$$

where $\mathbf{u}_0 = (0, 0, \dots, 0)$. This energy is convex and has a unique global minimum, which corresponds to the desired metric. Using Newton's method, the Yamabe energy can be optimized very efficiently. The Hessian matrix $H = (h_{ij})$ of the Yamabe energy has an explicit form. If $[v_i, v_j]$ is an edge on the mesh, $[v_i, v_j, v_k]$ and $[v_j, v_i, v_l]$ are the two faces adjacent to $[v_i, v_j]$, then $h_{ij} = \cot \theta_k^{ij} + \cot \theta_l^{ij}$, θ_k^{ij} is the corner angle at v_k in the face $[v_i, v_j, v_k]$. The diagonal element h_{ii} equals to $\sum_{j \neq i} h_{ij}$.

To compute a conformal mapping of a simply connected surface S , we set the target curvature to be zeros for all interior vertices, and the total curvature of boundary vertices to be 2π . For example, in order to map a human face surface to a rectangle, we select four corner vertices, and set their target curvatures to be $\frac{\pi}{2}$. The target curvatures for all other vertices are zeros. Using the Yamabe flow, we can obtain the desired metric. Then we flatten the mesh isometrically face by face using the resulting metric. Figure 2 shows two examples of conformal surface mappings using Yamabe flow method. The conformality is demonstrated using checkerboard texture mapping.

B. Quasi-conformal Map between Surfaces

After parameterizing the surfaces conformally, the next step is to determine a quasi-conformal registration between the conformal parameter domains. There may be important curves on the surfaces representing landmark features[24], so we look for the optimized harmonic diffeomorphism that exactly matches landmark features via a variational approach. However, minimizing the energy functional over the search space of landmark-matching surface diffeomorphisms is difficult. Following [10], we formulate our

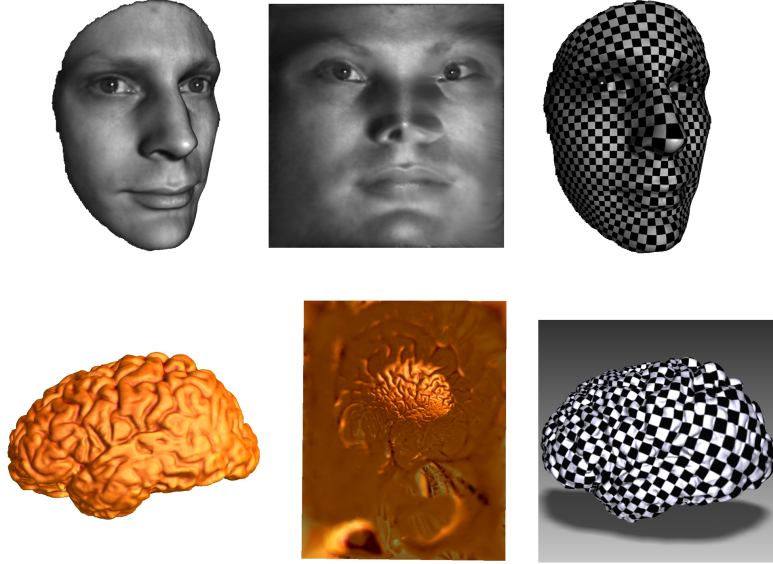


Fig. 2. Conformal mappings of a real human face and a real brain cortical surface, using Yamabe flow method. Four corners are picked, whose target curvatures are set to be $\frac{\pi}{2}$, and the target curvatures are set to be zeros everywhere.

problem as a variational energy defined on a search space of smooth vector fields \vec{V} . The diffeomorphism may then be generated through the integral flow of \vec{V} . \vec{V} are restricted only to those that do not flow across the landmark curves (to enforce exact landmark correspondence). Our energy has 2 terms: (1) a harmonic energy term to optimize the harmonicity of the parametrization maps; (2) a smoothness energy term to ensure the smoothness of the vector field.

Denote the conformal parameter domains of S_1 and S_2 by D_1 and D_2 respectively. We look for harmonic diffeomorphisms $\tilde{f}_1 : D_1 \rightarrow \Omega$ and $\tilde{f}_2 : D_2 \rightarrow \Omega$ that match landmark curves to a consistent location C . The composition map $\tilde{f}_2^{-1} \circ \tilde{f}_1$ is a landmark-matching harmonic diffeomorphism from D_1 to D_2 . To start with, we compute any arbitrary maps $f_{01} : D_1 \rightarrow \Omega$ and $f_{02} : D_2 \rightarrow \Omega$. We then iteratively look for the smooth vector field \vec{X}_i on Ω such that the composition map $\tilde{f}_i = \Phi^{\vec{X}_i} \circ f_{0i} : D_i \rightarrow \Omega$ is the landmark matching harmonic diffeomorphism ($i = 1, 2$). Here, $\Phi^{\vec{X}_i} : \Omega \rightarrow \Omega$ is the time-1 integral flow of the vector field $\vec{Y}_i = P_C \vec{X}_i$ satisfying the integral flow equation:

$$\begin{aligned} \frac{\partial \Phi^{\vec{X}_i}}{\partial t}(\mathbf{x}, t) &= \vec{X}_i(\Phi^{\vec{X}_i}(\mathbf{x}, t)), \\ \Phi^{\vec{X}_i}(\mathbf{x}, 0) &= \mathbf{x}. \end{aligned}$$

\vec{Y} is the projection of the vector field \vec{X}_i such that it is tangential to C . This ensures the exact landmark matching property of \tilde{f}_i .

The vector fields $\vec{X}_i = a_i \frac{\partial}{\partial x} + b_i \frac{\partial}{\partial y}$ minimizes the following energy functional:

$$\begin{aligned} J[a_i, b_i] &= \int_{\Omega} |\nabla \tilde{f}_1|^2 + |\nabla \tilde{f}_2|^2 dx + \lambda \int_C (\kappa_1(\tilde{f}_1) - \kappa_2(\tilde{f}_2))^2 ds_D \\ &\quad + \beta \int_{\Omega} |\nabla \vec{X}_1|^2 + |\nabla \vec{X}_2|^2 dx \end{aligned} \quad (7)$$

The variational problem is then formulated to be defined over the space of C^1 smooth vector fields on Ω . The last integral in the energy is the smoothness term for the vector fields \vec{X}_i . The first two integrals are

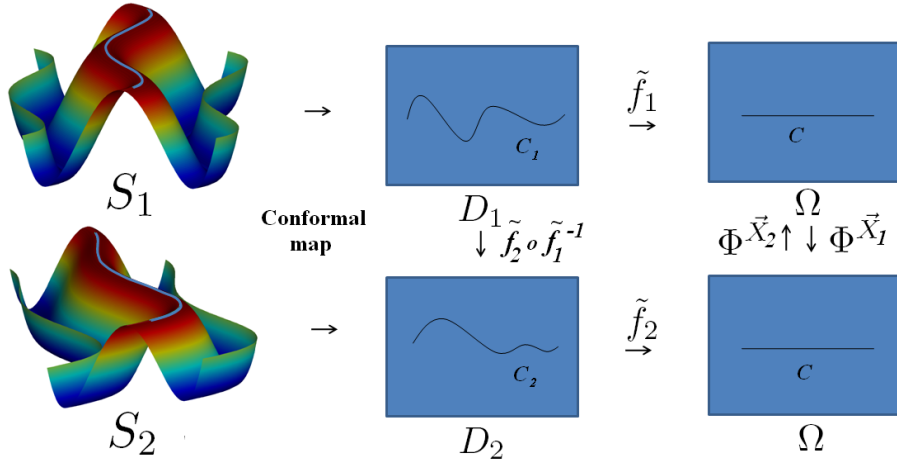


Fig. 3. How quasi-conformal registration is constructed between two surfaces.

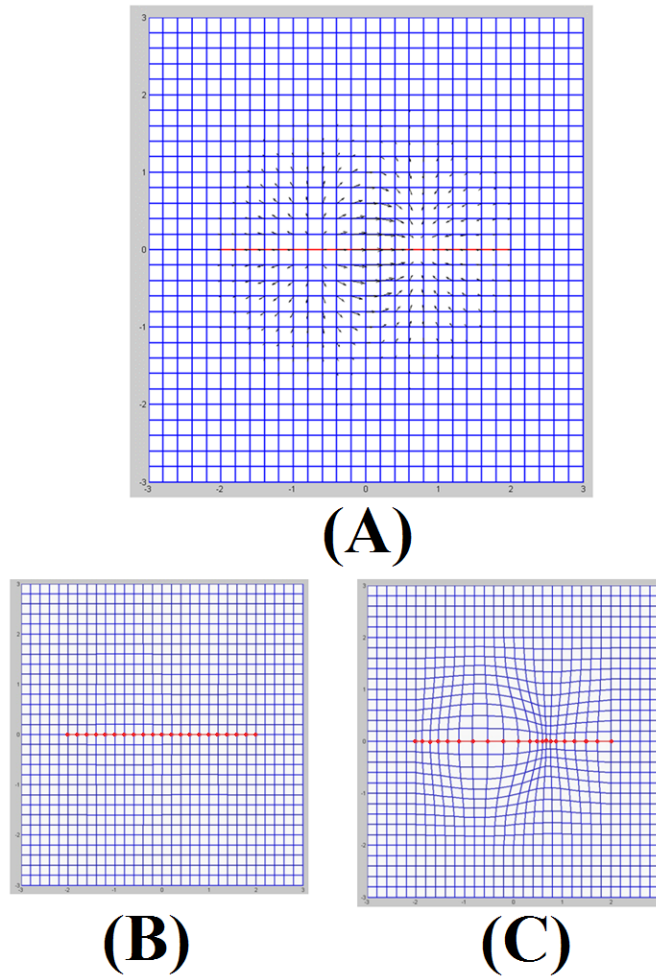


Fig. 4. (A) shows the vector field defined on the domain. The vector field on the landmark is tangential to the curve. (B) shows the grid lines on the domain. Several points are labeled on the landmark to visualize its displacement under the integral flow. (C) shows the result of the integral flow of the vector field. A diffeomorphism with exact landmark matching is obtained. Note that points slide along the landmark curve, instead of flowing across the curve.

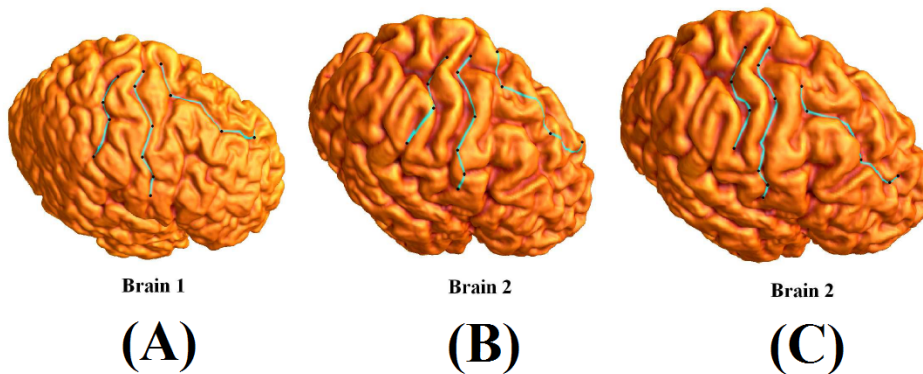


Fig. 5. Illustration of the result of matching the cortical surfaces with several sulcal landmarks. (A) shows brain surface 1. It is mapped to brain surface 2 under the conformal parameterization as shown in (B). (C) shows the result of matching under our proposed parameterization.

the harmonic terms, which aim to preserve the harmonicity of the parameterization as much as possible. The second term is a *symmetric* shape term defined as an arc length integral, where the shape measure is defined according to the curvature. The proposed energy functional can be minimized by modifying the vector field iteratively according to the following Euler-Lagrange equation:

$$\frac{da_i}{dt} = \int_0^1 B_i(\phi_s^{\bar{Y}_i}) \Psi_i(\phi_s^{\bar{Y}_i}, 1) \Psi_i^{-1}(\phi_s^{\bar{Y}_i}, s) P_C \bar{e}_1 |D\phi_s^{\bar{Y}_i}| ds - \beta \Delta a_i \quad (8)$$

$$\frac{db_i}{dt} = \int_0^1 B_i(\phi_s^{\bar{Y}_i}) \Psi_i(\phi_s^{\bar{Y}_i}, 1) \Psi_i^{-1}(\phi_s^{\bar{Y}_i}, s) P_C \bar{e}_2 |D\phi_s^{\bar{Y}_i}| ds - \beta \Delta b_i, \quad (9)$$

where:

$B_i := -\Delta \tilde{f}_i Df_{0,i} + \lambda \chi_A ((-1)^{i-1} (\kappa_1(\tilde{f}_1) - \kappa_2(\tilde{f}_2)) \nabla \kappa_i - \nabla \cdot C_i) Df_{0,i} |\nabla H(\phi)|$; Ψ_i is the orthogonal fundamental matrix for the homogeneous system of

$$\begin{aligned} \frac{\partial}{\partial t} P_i(x, t) &= \eta P_C \bar{e}_1 (\Phi^{\bar{Y}_i}(x, t)) + D\bar{Y}_i(\Phi^{\bar{Y}_i}(x, t)) P_i(x, t), \\ P_i(x, 0) &= \mathbf{0}. \end{aligned}$$

Figure 3 shows a schematic diagram of our quasi-conformal map construction. Figure 4 shows how the constraint vector field can be used to obtain the desired registration with exact landmark matching based on the shape information. Figure 5 illustrates the matching results for cortical surfaces with several sulcal landmarks labeled. Figure 5(A) shows brain surface 1 with several landmarks labeled. It is mapped to brain surface 2 under the conformal parameterization as shown in Figure 5(B). The sulcal landmarks on Brain 1 are only mapped approximately to the sulcal regions on Brain 2. Figure 5(C) shows the matching result under the parameterization we proposed. The corresponding landmarks are mapped exactly. Also, the correspondence between the landmark curves follows the shape information (corners to corners; see the black dot).

Using harmonic maps for registration is beneficial as they tend to preserve conformality as much as possible. They effectively capture the region of conformal deformation and help to identify regions of non-conformal deformation. By computing the Beltrami coefficient μ of the registration, we can detect abnormalities. In cases where the deformed surface does not undergo any abnormal (non-conformal) deformations, the harmonic map obtained will be close to conformal and μ will approximately be zero.

C. Computing the Beltrami coefficient

Given the conformal parameterizations together with the registration between the conformal parameter domains, we can detect the abnormal region by computing the Beltrami coefficient. The Beltrami coefficient measures the change in conformality. Suppose the conformal parameterizations of S_o and S_d are $\phi_o : S_o \rightarrow D_1$, $\phi_d : S_d \rightarrow D_2$ respectively. Denote the registration between the parameter domains by $F : D_1 \rightarrow D_2$. The composition map $\tilde{F} = \phi_d^{-1} \circ F \circ \phi_o : S_o \rightarrow S_d$ will give a landmark matching harmonic registration between the original and deformed surface. By computing the Beltrami coefficient $\mu_{\tilde{F}}$ of \tilde{F} , we can detect which point on the surface undergoes abnormal (non-conformal) deformation. The Beltrami coefficient is invariant under conformal maps. In other words, $|\mu_{f \circ g}| = |\mu_g|$ and $|\mu_{g \circ f}| = |\mu_f|$ if g is conformal. Since ϕ_o and ϕ_d are both conformal diffeomorphisms, we have:

$$|\mu_{\tilde{F}}| = |\mu_{\phi_d^{-1} \circ F \circ \phi_o}| = |\mu_F| \quad (10)$$

Thus, to compute $\mu_{\tilde{F}}$, it suffices to compute μ_F . Since F is a map defined on the 2D complex plane, we can compute its Beltrami coefficient easily by:

$$\mu_F = \frac{F_{\bar{z}}}{F_z} = \frac{\frac{\partial F}{\partial x} + i \frac{\partial F}{\partial y}}{\frac{\partial F}{\partial x} - i \frac{\partial F}{\partial y}} \quad (11)$$

The Beltrami coefficient is a complex-valued function. When the deformation near a point p is conformal, then $\mu_{\tilde{F}}(p) = 0$. At the point where abnormal deformation happens around its immediate neighborhood, $\mu_{\tilde{F}}$ will be non-zero. We can easily detect regions of abnormality by computing the norm of the Beltrami coefficient $|\mu_{\tilde{F}}|$.

To measure the degree of abnormality quantitatively, we introduce a measure called Beltrami Index (BI) which measures the average of the Beltrami coefficient over a certain region. Mathematically, it is defined as:

$$BI(D) = \int_D |\mu(z)| |dz| / \int_D |dz| \quad (12)$$

The Beltrami Index can effectively measure the degree of abnormalities in different regions on the surface (see Figure 17).

Also, as described in section 3, the argument of $\mu_{\tilde{F}}$ measures the angle of complex dilation. This can be used to describe any local rotational change of the abnormal shape. By representing $\mu_{\tilde{F}}$ as a vector field $\vec{V} = (\mathbf{Re}(\mu_{\tilde{F}}), \mathbf{Im}(\mu_{\tilde{F}}))$ on the parameter domain, we can easily visualize the rotational change of the abnormal shape (see Figure 9).

V. COMPUTER ALGORITHM

The computer algorithm can be summarized as follows:

- 1 Compute the conformal parameterizations of the original surface S_o and deformed surface S_d : $\phi_o : S_o \rightarrow D_1$ and $\phi_d : S_d \rightarrow D_2$;
- 2 Compute the landmark-matching harmonic registration between the conformal domains: $\tilde{F} : D_1 \rightarrow D_2$;

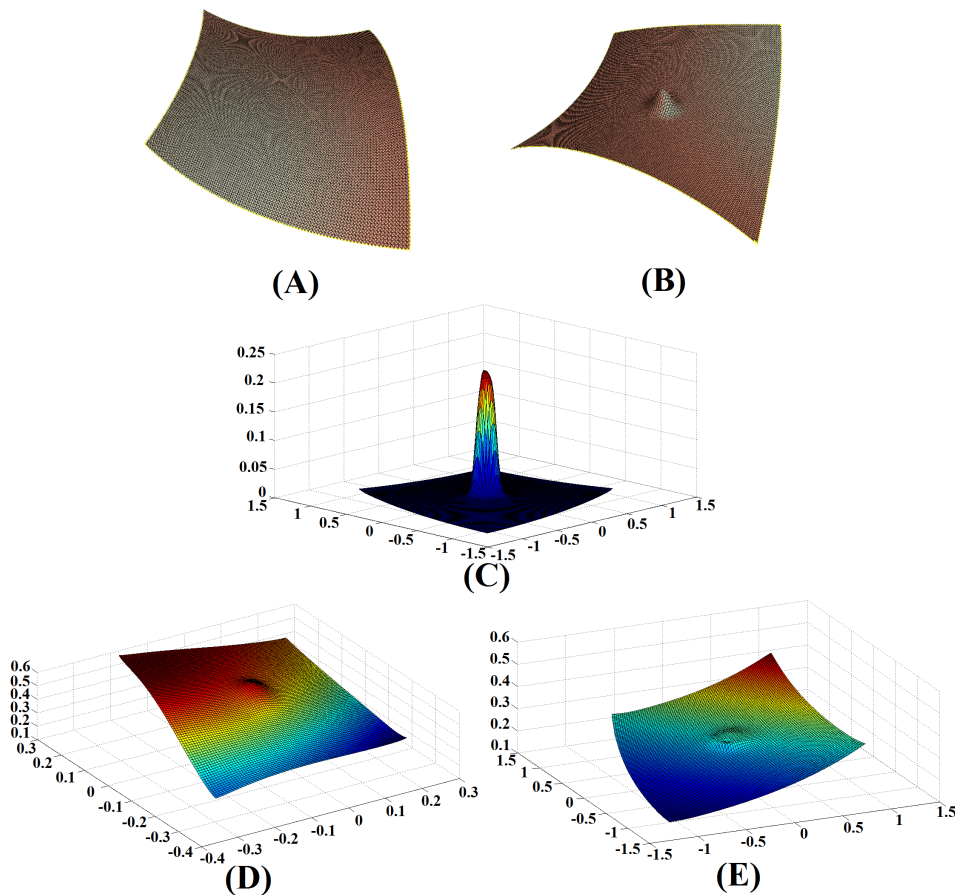


Fig. 6. (A) shows the original surface. (B) shows the deformed surface with both conformal and non-conformal deformations. (C) shows the plot of $|\mu|$. (D) shows the plot of the isometric indicator $|f^*(ds_E^2) - \text{Identity}|$. It is equal to 0 if f is isometric. (E) shows the gradient norm of the deformation field. Note that both the isometric indicator and the gradient of the deformation field are not good measures for detecting deformities.

- 3 Compute the Beltrami coefficient $\mu_{\tilde{F}}$ of \tilde{F} . Compute $|\mu_{\tilde{F}}|$ to detect regions of abnormality. The rotational change of the abnormal shape can be visualized by the vector field $\vec{V} = (\text{Re}(\mu_{\tilde{F}}), \text{Im}(\mu_{\tilde{F}}))$ on the parameter domain.

VI. EXPERIMENTAL RESULTS

We tested our proposed algorithm on synthetic surfaces, 3D human face data and MRI-derived models of human brain cortical surfaces, to detect abnormalities.

In Figure 6, we tested our proposed algorithm using synthetic data. Figure 6(A) shows the original surface. Figure 6(B) shows the deformed surface with both conformal and non-conformal deformations. Figure 6(C) shows the plot of $|\mu|$. It effectively detect the deformity on the surface. Figure 6(D) shows the plot of the isometric indicator $|f^*(ds_E^2) - \text{Identity}|$. It is equal to 0 if f is isometric. Figure 6(E) shows the gradient norm of the deformation field. Note that both the isometric indicator and the gradient of the deformation field are not good measures for detecting deformities. Figure 7 shows another example on synthetic surfaces. Figure 7(A) shows the original surface. Figure 7(B) shows the deformed surface with both conformal and non-conformal deformations. Figure 7(C) shows the plot of $|\mu|$. Figure 7(D)

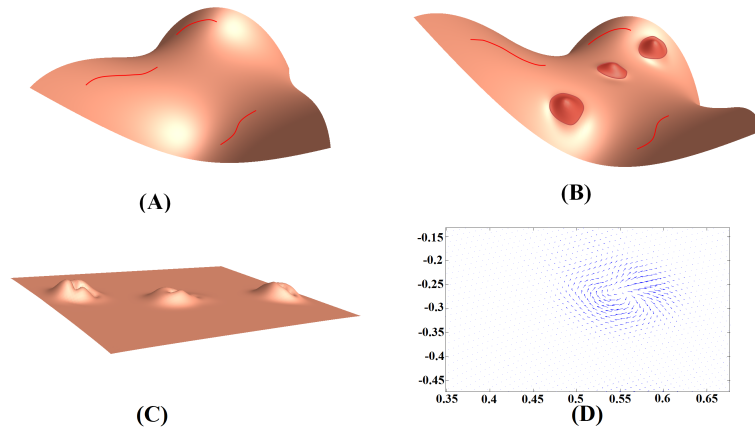


Fig. 7. (A) shows the original surface. (B) shows the deformed surface with both conformal and non-conformal deformations. (C) shows the plot of $|\mu|$. (D) shows the distribution of μ as a complex number. It represents a vector field on the conformal parameter domain. Observe that μ can be used effectively as an indicator to segment the abnormal regions on the surface.

shows the distribution of μ as a complex number. It represents a vector field on the conformal parameter domain- this can be used to visualize the rotational change of the abnormal shape. Again, it is observed that μ can be used effectively as an indicator to segment the abnormal regions on the surface (see the shaped segmented region on the surface in Figure 7(B)).

In Figure 8, we illustrate our idea on a human face. Figure 8(A) shows the original human face without abnormality. Figure 8(B) shows the deformed human face with abnormal swollen area. Figure 8(C) shows the the plot of $|\mu|$ versus the conformal parameter domain. Figure 8(D) shows the distribution of $|\mu|$ by color. Observe that μ can effectively reflect the swollen area on the human face.

Figure 9 shows how the complex-valued Beltrami coefficient μ can be used to detect rotational change of abnormal shape. It is done by visualizing μ as a vector field $\vec{V} = (\text{Re}(\mu_{\tilde{F}}), \text{Im}(\mu_{\tilde{F}}))$ on the parameter domain. Figure 9(A) shows a human face with an abnormally swollen area. In Figure 9(B), the swollen area is rotated. Figure 9(C) plots the complex-valued Beltrami coefficients μ on the parameter domain. Figure 9(D) shows the same area zoomed in. The green and red colors represent the Beltrami coefficients for (A) and (B), respectively. Observe that the Beltrami coefficients effectively reflect the rotational change of the swollen area. The abnormal shape is generally rotated by 90 degrees.

In Figure 10, we test our proposed algorithm on noisy data. Figure 10(A) shows the original clean human face. Figure 10(B) shows the deformed human face with noise. Figure 10(C) shows the original human face with noise. (D) shows the plot of μ computed under noise. Note that our method is stable under noise and can effectively detect deformities on noisy surface data.

In Figure 12, 13 and 14, we illustrate our proposed algorithm on a human brain cortical surface. Figure 12 shows the original brain surface (Brain 1) and the deformed brain surface (Brain 2) with abnormal gyral thickening. The gyral thickening can be observed inside the circled region. Figure 13 shows a zoom-in of the abnormal region. Gyral thickening is clearly observed. Figure 13(A) shows the plot of $|\mu|$ versus the parameter domain. Figure 13(B) shows the distribution of $|\mu|$ in color. Again, the Beltrami coefficient μ can effectively detect the gyral thickening region.

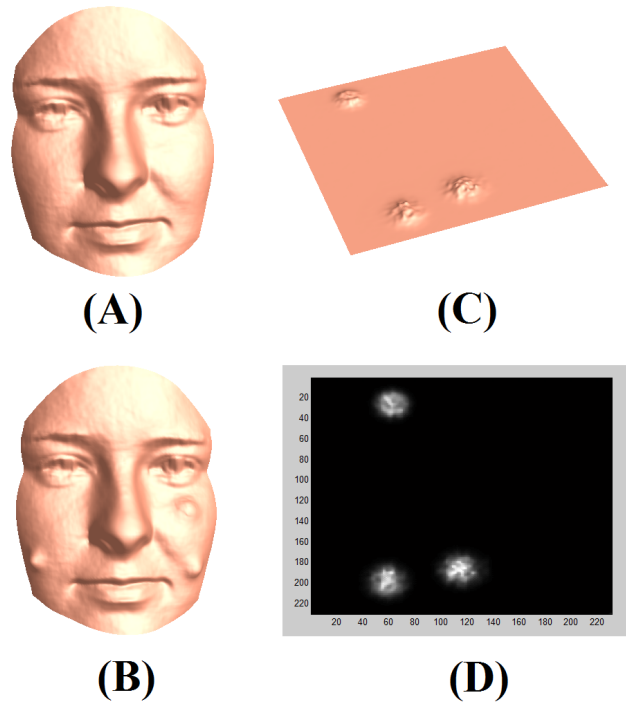


Fig. 8. (A) shows the original human face and (B) shows a deformed version of the human face with an abnormally swollen area. (C) shows the plot of $|\mu|$ versus the parameter domain. (D) shows the distribution of $|\mu|$ by color.

Figure 15 shows another example of detecting abnormalities on brain surfaces. Figure 15(A) shows the original brain surface. Figure 15(B) shows the deformed brain surface with gyral thickening in the circled regions. Figure 15(C) shows the distribution of $|\mu|$. The Beltrami coefficient μ again clearly reflects the region of abnormal changes on the human brain cortical surface.

Figure 16 illustrates how we can use Beltrami coefficient to capture the gyrification pattern on the human brain surface. Figure 16(A) shows a real human brain cortical surface. Figure 16(B) shows the deformed cortical surface. The brain has undergone different degrees of gyrification at different regions. Figure 16(C) shows the colormap of the brain determined by the Beltrami coefficient. Red color means high value of Beltrami coefficient whereas blue color means low value of Beltrami coefficient. Figure 16(D) shows the colormap on the conformal parameter domain. Observe that the colormap of the Beltrami coefficient effectively captures the gyrification pattern on the brain surface.

Figure 17 shows how we can qualitatively measure the degree of abnormalities using the Beltrami Index (BI). The top shows a series of brain surfaces which are undergoing more and more gyral thickening. The bottom shows the plot of the Beltrami Index (BI) of each deformed brain surfaces. Observe that the value of the Beltrami Index becomes bigger as the gyral thickening becomes more severe. It shows that the Beltrami Index (BI) can effectively measure the degree of the abnormal changes.

VII. CONCLUSION AND FUTURE WORK

In conclusion, we developed an effective algorithm to detect abnormalities on surfaces using quasi-conformal geometry. To do this, we computed a landmark-matching harmonic registration between the

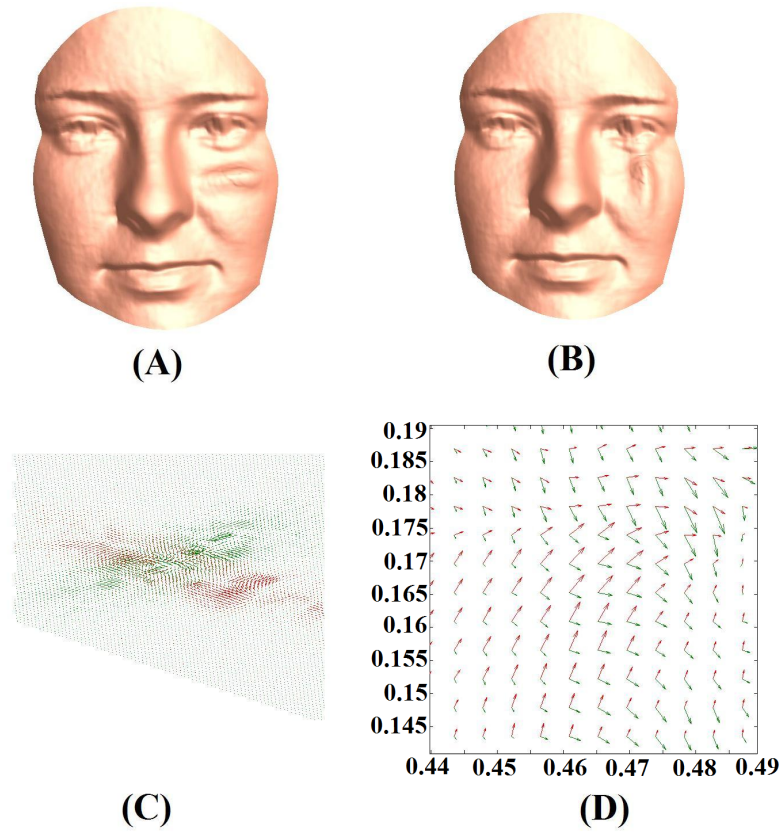


Fig. 9. (A) shows a human face with an abnormal swollen area. In (B), the swollen area is rotated. (C) plots the Beltrami coefficients μ on the parameter domain. (D) shows a zoomed-in region. The green and red colors represent the Beltrami coefficients for (A) and (B) respectively. Observe that the Beltrami coefficients effectively reflects the rotational change of the swollen area.

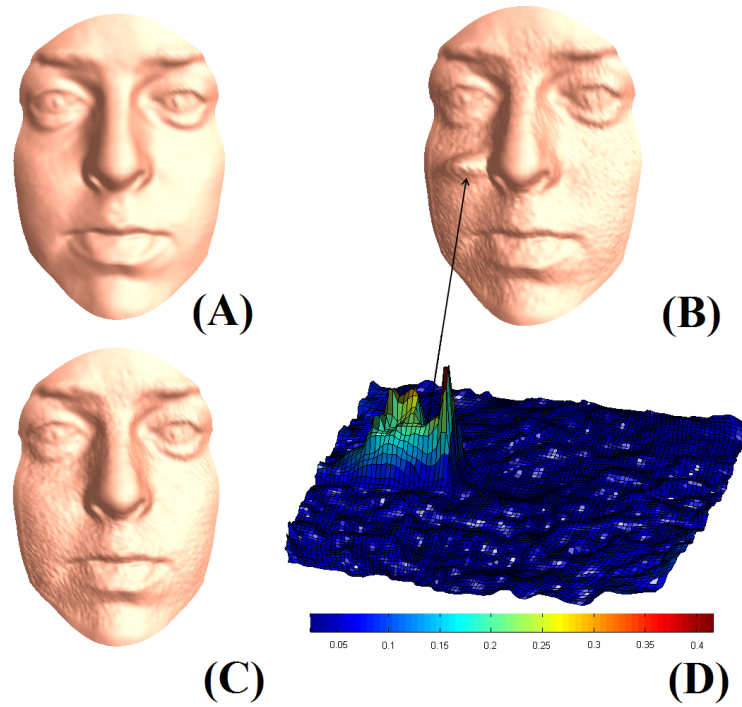


Fig. 10. (A) shows the original clean human face. (B) shows the deformed human face with noise. (C) shows the original human face with noise. (D) shows the plot of μ computed under noise.

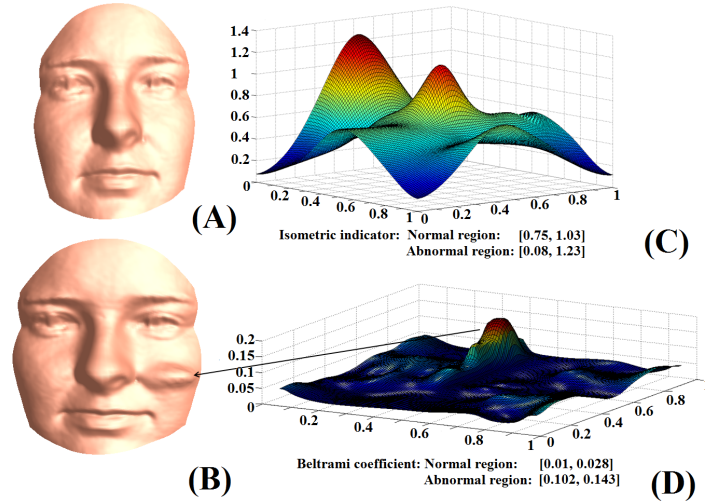


Fig. 11. (A) shows the original human face. (B) shows the deformed human face. The deformed face is fatter and abnormality is observed. The local geometry is well preserved (except for the abnormal region), although the face has become fatter. (C) shows the plot of the isometric indicator. (D) shows the plot of $|\mu|$.

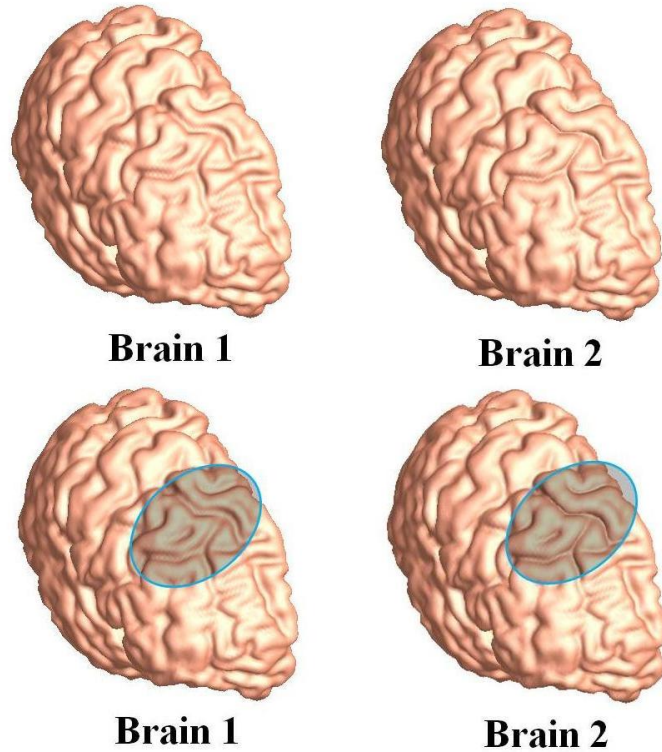
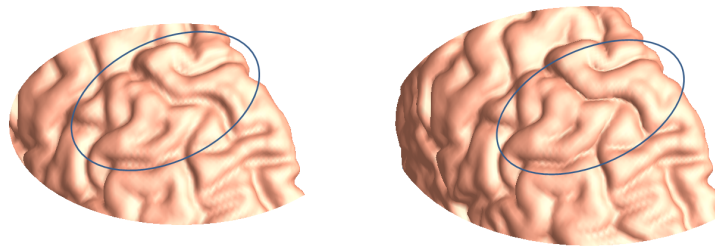


Fig. 12. The figure shows the original brain surface (Brain 1) and the deformed brain surface (Brain 2) with an abnormal thickening of the gyri, which can be observed inside the circled region.



Zoom in of the abnormal region.

Fig. 13. The figure shows a zoomed-in version of the abnormal region. Gyral thickening can be clearly observed.

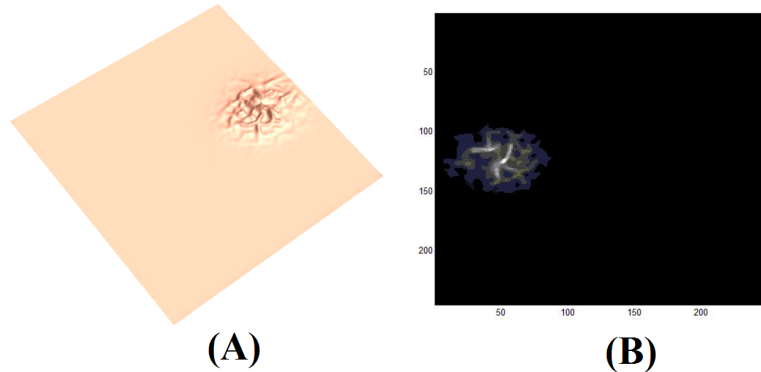


Fig. 14. (A) shows the plot of $|\mu|$ versus the parameter domain of the brain surfaces. (B) shows the distribution of $|\mu|$ by color.

original and deformed 3D surfaces, together with its associated Beltrami coefficient, μ . Experimental results show that the Beltrami coefficient can effectively detect regions with abnormalities, which are invariant under normal (conformal) deformation. By visualizing μ as a vector field defined on the parameter domain, we can capture the rotational change of the abnormal shape. In future, we will apply our algorithm to study human brain diseases such as Williams syndrome, which results from genetically-mediated developmental abnormalities in cortical folding. We will also develop more efficient numerical schemes to speed up the computation.

Acknowledgement: PT is supported by NIH: EB008432, EB008281, EB007813, HD050735 & AG036535. TC is supported by NSF GEO-0610079, NSF IIS-0914580, NIH U54 RR021813 and ONR N00014-09-1-0105. XG is supported by NIH 1R01EB0075300A1, NSF IIS 0916286, CCF0916235, CCF0830550, III0713145, and ONR N000140910228.

APPENDIX

Numerical Implementation of the Quasi-conformal Registration Algorithm

We describe how the quasi-conformal registration algorithm can be implemented. In practice, all surfaces are represented by meshes which consists of vertices, edges and triangular faces. The functions and their partial derivatives in the iterative scheme are defined on each vertex and linearly interpolated to define the value on each triangular face. They can be computed as follows:

- Laplacian of a function F can be computed as: $\Delta F = \sum_{[u,v] \in N_v} k_{uv}(F(v) - F(u))$, where: N_v is a set of triangles around v that forms a neighborhood of v ; $k_{uv} = (\cot \alpha + \cot \beta)/2$, where α and β

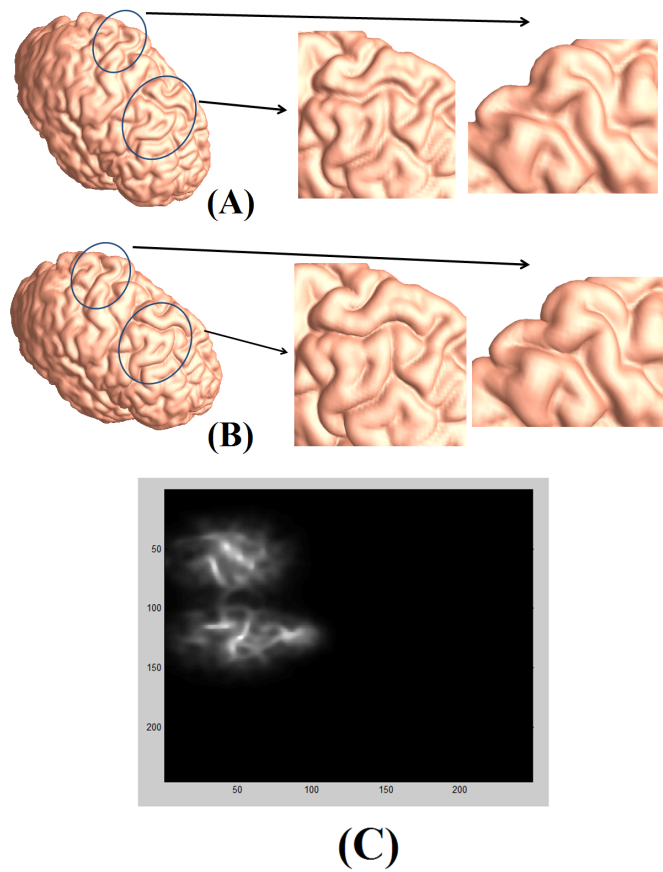


Fig. 15. The figure shows another example of detecting abnormalities on brain surfaces. (A) shows the original brain surface. (B) shows the deformed brain surface with gyral thickening inside the circled regions. (C) shows the distribution of $|\mu|$.

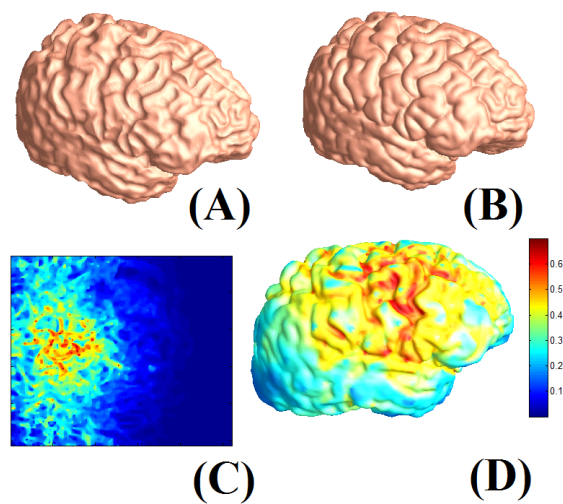


Fig. 16. (A) shows a real human brain cortical surface. (B) shows the deformed cortical surface. The brain has undergone different degrees of gyrification in different regions. (C) shows the colormap of the brain determined by the Beltrami coefficient. Red color indicates a high value of the Beltrami coefficient, whereas blue colors mean low values of Beltrami coefficient. (C) shows the colormap on the conformal parameter domain.

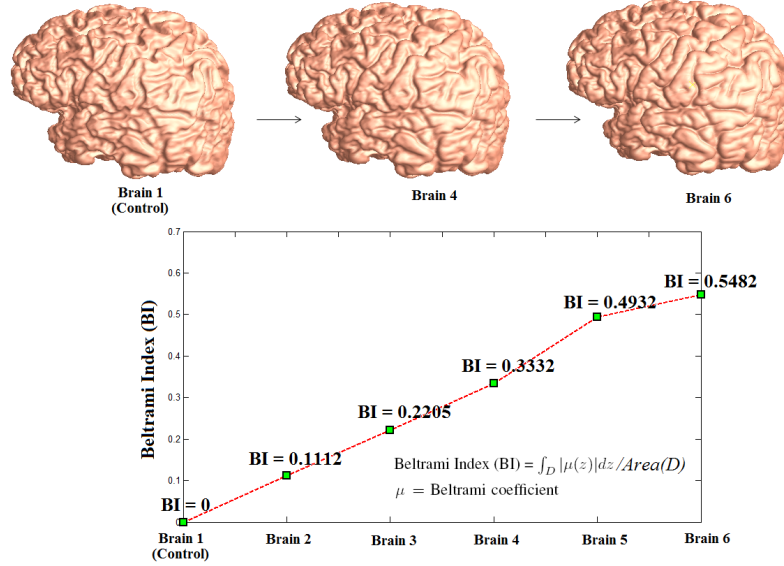


Fig. 17. The top shows a series of brain surfaces undergoing more and more gyri thickening. The bottom shows how the Beltrami Index (BI) can effectively measure the gyrification.

are the opposite angles of the edge $[u, v]$. For detail, please see [13].

- Gradient $\nabla \kappa_i$ can be computed as: $\nabla \kappa_i = \sum_{[u,v,w] \in N_v} \frac{\nabla_{[u,v,w]} \kappa_i}{n}$, where $\nabla_{[u,v,w]} \kappa_i$ is the gradient of κ_i on the triangle $[u, v, w]$. The value of κ_i on $[u, v, w]$ is linearly interpolated. n is the number of faces in N_v .
- $Df_{0,i}$ is defined as $Df_{0,i} = (\nabla f_{0,i}^1, \nabla f_{0,i}^2)$ which is a 2×2 matrix, where $f_{0,i} = (f_{0,i}^1, f_{0,i}^2)$. Similarly, $DY_i := (\nabla \vec{Y}_i^1, \nabla \vec{Y}_i^2)$, where $\vec{Y}_i = (Y_i^1, Y_i^2)$
- The orthogonal fundamental matrix $\Psi_i(\vec{x}, s)$ is defined as:
 $\Psi_i(\vec{x}, s) := \exp(\int_0^s D\vec{Y}_i(\Phi^{\vec{Y}_i}(\vec{x}, t)) dt)$. Suppose the interval $[0, 1]$ is discretized as: $s_0 = 0 < s_1 < \dots < s_n = 1$. $\Psi_i(\vec{x}, s)$ can be computed as: $\Psi_i(\vec{x}, s_k) := \exp(\sum_{j=1}^k D\vec{Y}_i(\Phi^{\vec{Y}_i}(\vec{x}, s_j))(s_j - s_{j-1}))$.
- The function δ_ϵ is defined to be a positive function that is compactly supported in $(-\epsilon, \epsilon)$ and can be computed mathematically as:

$$\delta_\epsilon(x) = \frac{1}{a(\epsilon)\sqrt{\pi}} \exp\left(-\frac{x^2}{a(\epsilon)^2}\right)$$
- η_{ep} is a smooth function on Ω such that $\eta_{ep} = 0$ at the endpoints of the open curves $\Gamma_k \subset C$, $k = 1, 2, \dots, N$. It can be computed mathematically as: $\eta_{ep} = 1 - \sum_{i=1}^{2N} \delta_\epsilon^i(x)$, where $\delta_\epsilon^i(x) = \exp(-(x - a_i)/\epsilon^2)$ and a_1, a_2, \dots, a_{2N} are the set of end points of the landmark curves.
- The initial map $f_{0,i}$ maps the landmark curves C_i to the common curve $C_{standard,i}$. It can be computed as follows: Given a set of landmark curves $C_i(t)$ on the parameter domain and a set of corresponding common curves $C_{standard,i}(t)$. Starting from the initial map $f_0 = \text{Id}$, we can iteratively flow the map to get a diffeomorphism which matches $C_i(t)$ to $C_{standard,i}(t)$ as follow. We can define a vector fields on $f^n(C_i(t))$ as $\vec{V}^n(t) = C_{standard,i}(t) - f^n(C_i(t))$ and smoothly extend to the parameter domain by Gaussian convolution $G * \vec{V}^n(t)$. The iterative scheme can then be written as: $f^{n+1} = f^n + dt \vec{V}_n(f^n)$.

REFERENCES

- [1] (MR2015261) B. Chow and F. Luo. Combinatorial Ricci flows on surfaces. *Journal of Differential Geometry*, **63**(2003), 97-129.
- [2] M. K. Chung, K. J. Worsley, S. Robbins, T. Paus, J. Taylor, J. N. Giedd, J. L. Rapoport, , and A. C. Evans. Deformation-based surface morphometry applied to gray matter deformation. *NeuroImage*, **18**(2003), 198-213.
- [3] C. Gaser, H.-P. Volz, S. Kiebel, S. Riehemann, and H. Sauer. Detecting structural changes in whole brain based on nonlinear deformations—application to Schizophrenia research. *NeuroImage*, **10**(1999), 107-113.
- [4] U. Grenander and M. I. Miller. Computational anatomy: An emerging discipline. *Quarterly of Applied Mathematics*, **56**(1998), 617-694.
- [5] X. Gu, S. Wang, J. Kim, Y. Zeng, Y. Wang, H. Qin, and D. Samaras. Ricci flow for 3D shape analysis. *Proceedings of IEEE International Conference on Computer Vision*(2007), 1-8.
- [6] X. Gu, Y. Wang, T. F. Chan, P. M. Thompson, and S.-T. Yau. Genus zero surface conformal mapping and its application to brain surface mapping. *IEEE Transaction on Medical Imaging*, **23**(2004), 949-958.
- [7] (MR0954419) R. S. Hamilton. The Ricci flow on surfaces. *Mathematics and General Relativity (Santa Cruz, CA, 1986)*, *Contemporary Mathematics, American Mathematics Society* **71**(1988), 237-262.
- [8] N. A. Lord, J. Ho, and B. C. Vemuri. USSR: A unified framework for simultaneous smoothing, segmentation, and registration of multiple images. *IEEE 11th International Conference on Computer Vision*, (2007), 1-6.
- [9] N. A. Lord, J. Ho, B. C. Vemuri, and S. Eisenschenk. Simultaneous registration and parcellation of bilateral hippocampal surface pairs for local asymmetry quantification. *IEEE Transaction on Medical Imaging*, **26**(2007), 471-478.
- [10] L. M. Lui, S. Thiruvankadam, Y. Wang, T. Chan, and P. Thompson. Optimized conformal parameterization of cortical surfaces using shape based matching of landmark curves. *SIAM Journal of Imaging Sciences*, , **3**(2010), 52-78.
- [11] L. M. Lui, Y. Wang, T. F. Chan, and P. Thompson. Landmark constrained genus zero surface conformal mapping and its application to brain mapping research. *Applied Numerical Mathematics*, **57**(2007), 847-858.
- [12] (MR2100762) F. Luo. Combinatorial Yamabe flow on surfaces. *Communications in Contemporary Mathematics*, **6**(2004), 765-780.
- [13] (MR1246481) U. Pinkall and K. Polthier. Computing discrete minimal surfaces and their conjugates. *Experimental Mathematics*, **2**(1993), 15-36.
- [14] K. M. Pohl, J. Fisher, W. E. L. Grimson, R. Kikinis, and W. M. Wells. A Bayesian model for joint segmentation and registration. *NeuroImage*, **31**(2006), 228-239.
- [15] Y. Shi, A. L. Reiss, A. D. Lee, R. A. Dutton, U. Bellugi, A. M. Galaburda, J. R. Korenberg, D. L. Mills, I. Dinov, P. M. Thompson, and A. W. Toga. Hamilton-Jacobi skeletons on cortical surfaces with applications in characterizing the gyrification pattern in Williams Syndrome. *IEEE International Symposium on Biomedical Imaging*, (2007), 660-663.
- [16] Y. Shi, P. M. Thompson, I. Dinov, S. Osher, and A. W. Toga. Direct cortical mapping via solving partial differential equations on implicit surfaces. *Medical Image Analysis*, **11**(2007), 207-223.
- [17] P. Thompson, J. Giedd, R. Woods, D. MacDonald, A. Evans, and A. Toga. Growth patterns in the developing brain detected by using continuum-mechanical tensor maps. *Nature*, **404-6774**(2000), 190-193.
- [18] D. Tosun, A. L. Reiss, A. D. Lee, R. A. Dutton, K. M. Hayashi, U. Bellugi, A. M. Galaburda, J. R. Korenberg, D. L. Mills, A. W. Toga, and P. M. Thompson. Use of 3-D cortical morphometry for mapping increased cortical gyrification and complexity in Williams Syndrome. *IEEE International Symposium on Biomedical Imaging*, (2006), 1172-1175.
- [19] G. Unal and G. Slabaugh. Coupled PDEs for non-rigid registration and segmentation. *IEEE Conference on Computer Vision and Pattern Recognition*, **1**(2005), 168-175.
- [20] M. Vaillant, M. I. Miller, L. Younes, and A. Trouvé. Statistics on diffeomorphisms via tangent space representations. *NeuroImage*, **23**(2004), S161-S169.
- [21] Y. Wang, L. M. Lui, T. F. Chan, and P. M. Thompson. Optimization of brain conformal mapping with landmarks. *8th International Conference on Medical Image Computing and Computer Assisted Intervention*, (2005), 675-683.
- [22] W. Zeng, X. Yin, Y. Zeng, Y. Lai, X. Gu, and D. Samaras. 3D face matching and registration based on hyperbolic Ricci flow. *CVPR 3D Face Processing Workshop*, (2008), 1-8.
- [23] W. Zeng, Y. Zeng, Y. Wang, X. Yin, X. Gu, and D. Samaras. 3D non-rigid surface matching and registration based on holomorphic differentials. *European Conference on Computer Vision*, (2008), 1-14.
- [24] L.M. Lui, Y. Wang, T.F. Chan, and P.M. Thompson. Brain Anatomical Feature Detection by Solving Partial Differential Equations on General Manifolds *Discrete and Continuous Dynamical Systems B*, **7**(2007), 605-618.
- [25] Y. Wang, L. M. Lui, X. Gu, K.M. Hayashi, T.F. Chan, P.M. Thompson, and S.-T. Yau. Brain Surface Conformal Parameterization using Riemann Surface Structure *IEEE Transaction on Medical Imaging*, **26**(2007), 853-865.